Dalton Transactions

ROYAL SOCIETY OF CHEMISTRY

PAPER

Check for updates

Cite this: *Dalton Trans.*, 2020, **49**, 1822

High performance MIL-101(Cr)@6FDA-*m*PD and MOF-199@6FDA-*m*PD mixed-matrix membranes for CO_2/CH_4 separation†

Alexander Nuhnen,[a] Maximilian Klopotowski,[a] Harold B. Tanh Jeazet,[a] Sara Sorribas,[b] Beatriz Zornoza,[b,c] Carlos Téllez,[b] Joaquín Coronas *[b] and Christoph Janiak *[a]

Received 7th August 2019,
Accepted 13th January 2020

DOI: 10.1039/c9dt03222c

rsc.li/dalton

Combination of the polyimide 6FDA-*m*PD (6FDA = 4,4′-hexafluoroisopropylidene diphthalic anhydride and *m*PD = *m*-phenylenediamine) and crystallites of the metal–organic frameworks (MOFs) MIL-101(Cr) or MOF-199 (HKUST-1, Cu-BTC) produces mixed-matrix membranes (MMMs) with excellent dispersion and compatibility of the MOF particles within the polymer matrix. Permeation tests of a binary CO_2/CH_4 (50/50) gas mixture showed a remarkable increase of CO_2 permeabilities for MIL-101(Cr)@6FDA-*m*PD and significantly higher selectivities for MOF-199@6FDA-*m*PD. The CO_2 permeability increased from 10 (neat polymer) to 50 Barrer for the 24 wt% MIL-101(Cr)@6FDA-*m*PD membrane (with essentially constant selectivity) due to the high pore volume of MIL-101(Cr). The CO_2/CH_4 selectivity increased from 54 to 89 from the neat 6FDA-*m*PD polymer to the 24 wt% MOF-199@6FDA-*m*PD membrane, apparently due to the high CO_2 adsorption capacity of MOF-199.

Introduction

Membrane technology plays an important role in the reduction of the environmental impact and operational costs of industrial separation processes as energy costs increase. As a result, application of membrane technology can help to save energy up to 50% of the production costs.[1,2] As the ratio between equipment size and production capacity decrease, membrane technologies address the requirements of process intensification.[3] Distillation and absorption-based processes are among conventional technologies that require a phase change in the mixture to be separated. This phase change increases significantly the energy loss which may be avoided in the case of membrane gas separation which does not require a phase change.[4] Separation through membranes is mainly based on the size and shape of the molecules to be separated and on their interaction with the membrane material.[5] The commercially applied membrane materials are mostly made from polymers. These are cheaper to produce and easier to process as flat sheet or hollow fiber membranes than inorganic materials.[6]

The most basic requirements for choosing membrane materials are the selectivity and the permeability parameters. These can be mainly used to determine the economic performance of membrane processes.[7] From this point of view, the existing polymeric membrane materials are not optimal: improvement in permeability is always at the expense of selectivity, and *vice versa*.[8] Also plasticization hinders the application of polymeric membranes at high pressures since the swelling and dilatation of the polymer due to high concentration of adsorbates may induce an increase in the mobility of the polymer chains and therefore reduce the membrane selectivity.[6]

To improve the performance of polymeric membranes several solutions have been proposed during the last decades. Various polymers have been modified using different types of inorganic additives such as zeolites, mesoporous silicas, activated carbons, carbon nanotubes and non-porous solids to produce mixed-matrix membranes (MMMs).[7,9–20] MMMs are composite membranes consisting of micro- or nanoparticles of an inorganic or inorganic–organic hybrid material (dispersed phase) incorporated into a polymer matrix (continuous phase). Polymer, filler properties, filler loading and homogeneous dispersion affect the MMM morphology as well as the separation performance.[7,13] The chemical structure, surface chemistry, particle size distribution and aspect ratio are key parameters

[a]*Institut für Anorganische Chemie und Strukturchemie, Heinrich-Heine-Universität Düsseldorf, 40204 Düsseldorf, Germany. E-mail: janiak@hhu.de*
[b]*Chemical and Environmental Engineering Department, Instituto de Nanociencia de Aragon, Instituto de Ciencia de Materiales de Aragón (ICMA), Universidad de Zaragoza-CSIC, 50018 Zaragoza, Spain. E-mail: coronas@unizar.es*
[c]*Department of Energy and Environment, Instituto de Carboquímica-ICB-CSIC, Miguel Luesma Castán 4, 50018 Zaragoza, Spain*

†Electronic supplementary information (ESI) available: TGA, PXRDs, SEM-EDX, Maxwell model, permeation data, T_g. See DOI: 10.1039/c9dt03222c

of the filler. MMMs may provide separation properties which can be above the so-called Robeson upper bound.[18]

Recent advances have shifted towards the use of metal organic frameworks (MOFs) as potential fillers in the polymer matrix.[21] MOFs exhibit advantages over zeolites and therefore are potential additives for deep impact in MMM separation properties.[22–27] For example, because of the broad variety of functionalities of organic ligands in MOFs, they can interact strongly with the polymer phase, so that the volume of micro gaps between inorganic and organic phase, which cause loss in selectivity, can be diminished.[12–14] To obtain materials with optimized separation properties a perfect interaction between the two components has to be established for the preparation of MMMs together with a good dispersion avoiding as much as possible filler agglomeration. In addition, MOFs are not only tuneable concerning their chemical groups, but also for their textural properties (pore volume and surface area).[28] Therefore, the MOF effect on the membrane properties can be higher for a given mass loading than that corresponding to conventional fillers. As emphasized in theoretical predictions, the choice of suitable MOF/polymer pairs is necessary for high-performance MMMs in addition to the control of interface morphology.[29]

Different to the studies made on continuous (pure) MOF membranes[24,26,30] we present herein results on the CO_2/CH_4 separation with MMMs of MIL-101(Cr)[31] or MOF-199 (also named HKUST-1 or Cu-BTC)[32] with the polyimide 6FDA-*m*PD (Scheme 1) (6FDA = 4,4′-hexafluoroisopropylidene diphthalic anhydride and *m*PD = *m*-phenylenediamine). The neat polyimide 6FDA-*m*PD is thermally stable until about 500 °C (Fig. S1 in ESI†) and shows excellent mechanical stability.[33] Furthermore, 6FDA-*m*PD features good properties in both permeation and selectivity for CO_2/CH_4 separation processes.[33]

The CO_2 sorption of MOFs has been the subject of intense interest for "carbon capture".[34] MIL-101(Cr) exhibits a moderate CO_2 uptake of 10.5 wt% (1 bar, 293 K),[35] while MOF-199 is one of the best MOFs for CO_2 adsorption with an uptake capacity of 27 wt% (1 bar, 298 K).[36]

Even though it has been shown in the last years that several MOFs are very interesting for the fabrication of MMMs with very attractive separation characteristics (see Table S5 in ESI† for some specific examples),[9,10,12,13] the separation performance of the present study is remarkable. Particularly, we present here MOF-containing gas-separation membranes with technologically attractive properties.

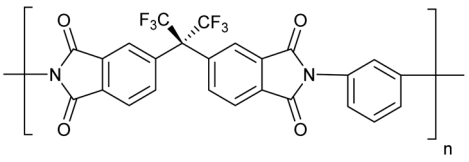

Scheme 1 6FDA-*m*PD repeating unit (6FDA = 4,4′-hexafluoroisopropylidene diphthalic anhydride and *m*PD = *m*-phenylenediamine).

Experimental

Materials and methods

Chromium nitrate nonahydrate ($Cr(NO_3)_2{\cdot}9H_2O$, 99%) hydrofluoric acid (analysis grade), toluene (>99%) and triethylamine (99%) were obtained from Acros Organics. Methanol (99.8%), *m*-phenylenediamine (*m*PD, 99%) and acetic anhydride (>97%) were acquired from fisher scientific. Copper acetate monohydrate $Cu(OAc)_2{\cdot}H_2O$, (99%) was purchased from Aldrich. Benzene-1,3,5-tricarboxylic acid (H_3BTC, 99%) and benzene-1,4 dicarboxylic acid (H_2BDC, 98%) were acquired from Aldrich. 4,4′-Hexafluoroisopropylidene diphthalic anhydride (6FDA, >98%) and *N*,*N*-dimethyl acetamide (DMAc, >99%) were obtained from TCI. Dichloromethane (DCM, >99.9%), *N*,*N*-dimethylformamide (DMF, 99.9%) and ethanol (99.9%) were purchased from Prolabo. Gases CO_2 and CH_4 were supplied by Air Liquide (Germany) and used as received (purity 99.995%).

Powder X-ray diffraction patterns (PXRD) were obtained on a Bruker D2 Phaser powder diffractometer with a flat silicon, low background sample holder, at 30 kV, 10 mA for Cu-Kα radiation (λ = 1.5418 Å). In all diffractograms, the most intense reflection was normalized to 1.

Nitrogen sorption isotherms were measured at 77 K using a Quantachrome Autosorb iQ MP gas sorption analyzer. Ultra-high purity (UHP, grade 5.0, 99.999%) nitrogen, and helium gases were used; the latter was used for performing cold and warm free space correction measurements. MIL-101(Cr) and MOF-199 BET surface areas (2770 $m^2\ g^{-1}$ and 950 $m^2\ g^{-1}$, respectively) and pore sizes were calculated using sample weights after degassing for 2 h at 150 °C with the built-in oil-free vacuum system of the instrument (ultimate vacuum $<10^{-8}$ mbar).

To acquire scanning electron microscopy (SEM) images alone, the MOF particles and the membrane cross-sections were coated with gold. The cross sections were obtained by breaking the membranes after freezing in liquid nitrogen. The coated samples were then imaged using an ESEM Quanta 400 FEG SEM equipped with a secondary electron (SE) detector and operated at 20 keV.

The MIL-101(Cr) microcrystals were coated with palladium and the SEM image was obtained on Zeiss Leo DSM 982 Gemini with field emitter.

SEM images combined with EDX-mapping were recorded with a Jeol JSM-6510LV QSEM Advanced electron microscope with a LAB-6 cathode at 20 keV. The microscope was equipped with a Bruker Xflash 410 silicon drift detector and the Bruker ESPRIT software for EDX analysis. The membrane cross-sections were prepared through freeze-fracturing after immersion in liquid nitrogen and then coated with gold by a Jeol JFC 1200 fine-coater at an approximate current of 20 mA for 20–30 s.

Differential scanning calorimetry (DSC) was measured using a Mettler Toledo DSC 3 with a temperature gradient of 10 K min^{-1} in the temperature range of 20 °C to 400 °C for the determination of the glass temperatures (T_g). All samples were heated four times and cooled 3 times. The glass temperature

was determined as the mean of the 2nd and 3rd heating and cooling cycle. The results were analyzed with the STARe SW 16.00 Software.

Synthetic procedures

MIL-101(Cr). MIL-101(Cr) was synthesized according to the previously reported procedure.[31] A typical synthesis involved a solution containing chromium(III) nitrate $Cr(NO_3)_3{\cdot}9H_2O$ (400 mg, 1 mmol), hydrofluoric acid (1 mmol) and 1,4-benzene dicarboxylic acid H_2BDC (164 mg, 1 mmol) in 5 mL of H_2O. The mixture was transferred to the Teflon line in a hydrothermal autoclave which was heated for 6 h at 210 °C and cooled afterwards slowly to room temperature over a time period of 8 h. The mixture was then isolated from the autoclave and the solid separated from the solution through centrifugation (4200 U min^{-1} for 50 min). A significant amount of recrystallized terephthalic acid was present. To eliminate most of the carboxylic acid, the product was dispersed and centrifuged two times in DMF (20 mL), one time in ethanol (10 mL) and one time in water (10 mL). The final product was then dried at room temperature (yield 302 mg, 50%).

MOF-199 (HKUST-1, Cu-BTC). The synthesis was carried out according to the procedure reported by Tranchemontagne *et al.*[32] Benzene-1,3,5-tricarboxylic acid (514 mg, 2.40 mmol) and $Cu(OAc)_2{\cdot}H_2O$ (817 mg, 4.37 mmol) were dissolved each in 12 mL of a 1 : 1 : 1 mixture of H_2O/DMF/EtOH. Both solutions were mixed together and the resulting mixture was stirred for about 30 min. After addition of 0.5 mL of triethylamine, the solution was stirred for 6 days. The obtained turquoise suspension was poured on 100 mL of DMF and allowed to stand overnight, afterwards it was centrifuged at 2000 rpm for 99 min and the supernatant was removed. This washing procedure was repeated three times. The product was collected, immersed in 100 mL of CH_2Cl_2, left overnight and centrifuged as given above. This last washing step was also repeated three times and afterwards the product was dried overnight under vacuum (yield: 430 mg, 59%). We choose this synthetic procedure to yield especially small MOF particles in the submicrometer range. Because of the subsequent use in mixed-matrix membranes particle size is of prime importance for a defect free composite membrane.

6FDA-*m*PD. The synthesis was carried out according to the procedure reported by Staudt-Bickel and Koros[33] All monomer materials were purified before the polymerization reaction. 6FDA (4,4′-hexafluoroisopropylidene diphthalic anhydride) was sublimed twice; *m*PD (*m*-phenylenediamine) was recrystallized twice from toluene. The monomers were stored separately under high vacuum. For the synthesis of the polyimide in this study, chemical imidization was performed. In a moisture free flask with nitrogen inlet and magnetic stirrer, the diamine monomer was dissolved in *N*,*N*-dimethyl acetamide (DMAc) and the 6FDA dianhydride dissolved in DMAc was added dropwise at room temperature. The 20–25 wt% solution was stirred 6–8 h. Thereby high molecular polyamic acids were formed. The imidization was performed by the dehydration of the polyamic acids by adding a large excess of triethylamine and acetic anhydride to the reaction mixture and stirring for 2–3 h at 323 K and 10–20 min at 373–383 K. After cooling to room temperature, the highly viscous reaction solution was slowly poured into methanol. The precipitated polyimide (6FDA-*m*PD) was homogenized in a blender; filtered and washed several times with fresh methanol. The obtained polyimide was dried 12 h under vacuum at room temperature and at least 24 h under vacuum at 523 K.

Mixed-matrix membranes. 500 mg of the polymer (6FDA-*m*PD) was dissolved in 7 mL dichloromethane (CH_2Cl_2) and the solution was stirred for 24 h. For an 8 wt% MMM simultaneously 44 mg of the MOF material (MIL-101(Cr) or MOF-199) was suspended in 9 mL CH_2Cl_2 and stirred for 24 h (44/(500 + 44) × 100% = 8%). Next the MOF suspension was homogenized by ultrasonication for which the sample was treated three times for 15 min each with an amplitude of 20% by an ultrasonic liquid processor (VCX 750 Sonics, Microtip 630-0419). Then a small portion of the polymer solution was added to the MOF suspension. After further stirring for 24 h, the ultrasonication procedure was repeated. Then the remaining polymer solution was added. Before casting, the dispersion was kept under stirring for one hour. The dispersion was cast into metal rings, 4 cm in diameter, which were placed on a flat stainless-steel surface. All of the casting equipment was placed on top of an adjustable table to assure horizontal alignment during the membrane formation. To prevent contamination by dust particles and to ensure a slow evaporation of the solvent, a funnel was placed upside down over the metal ring and the small opening was covered with filter paper. As soon as all solvent had evaporated, the membrane was removed from the metal ring and the stainless-steel surface by flushing the ring with distillated water. The membrane was finally dried in a vacuum oven at 120 °C and 50 mbar overnight. MMMs with 16 and 24 wt% were produced the same way with 95 mg and 158 mg MOF material (MIL-101(Cr) or MOF-199), respectively. The pure polymer membranes were prepared accordingly and dried the same way.

We also tried to produce MMMs with loadings of above 24 wt% MOF. Unfortunately, the MMMs with filler loadings of above 24 wt% were to brittle for handling and gas separation measurements. The MMMs either broke after casting or while preparing them for the measurement. Therefore, we are not able to prepare defect-free membranes and to present separation performance data of MMMs with filler loadings above 24 wt%.

Gas permeation experiments

Conducted in Spain, Zaragoza. A detailed description of the gas permeation setup can be found elsewhere.[37] The membranes (13.8 cm^2) were placed inside a permeability module composed of two stainless steel parts with a cavity in which a macroporous disk support (20 μm nominal pore size, Mott Corp.) is gripped inside with Viton O-Rings. Mass-flow meter controllers (Alicat Scientific) were used for feed and sweep gas

provision to the membrane module. A CO_2/CH_4 (25/25 cm^3 (STP) min^{-1}) mixture stream was fed at 3 bar to the retentate side, while the permeate side was swept with a 2 cm^3 (STP) min^{-1} mass-flow controlled stream of Ar at 1 bar. Gas concentrations in the outgoing stream were analyzed by an Agilent 3000A on-line gas micro-chromatograph equipped with thermal conductivity detector (TCD). Permeability results in Barrer (1×10^{-10} cm^3 (STP) cm (cm^2 s cmHg)$^{-1}$) were obtained once the exit stream of the membrane was stabilized. The real separation selectivity of the mixtures was calculated as the ratio of permeabilities. Permeation measurements were performed at 35 °C controlled by a Memmert UNE 200 oven.

Conducted in Germany, Düsseldorf. Binary gas separation experiments were carried out with a continuous flow permeation system (OSMO inspector, provided by Convergence Industry B.V., 7532 SM Enschede, The Netherlands) with helium as sweep gas and an Agilent 490μGC gas chromatograph to measure the gas concentration in the permeate. The membranes were cut in a round sheet, placed in the permeation module (4.5 cm diameter) and covered by a rubber ring to provide an effective inner diameter of 3.8 cm with an area of 11.3 cm^2. All permeation experiments were performed at 25 °C and with 3 bar transmembrane pressure. The feed gases were mixed in a 50/50 volume flow mixture of CO_2 and CH_4 by two Bronkhorst Coriolis-flow controllers as well as the helium gas stream with a total upstream flow of 160 mL min^{-1}. The downstream is swept with helium at a rate of 1 mL min^{-1} at ambient pressure. The gas concentration in the permeate stream was measured with the Agilent 490μGC with a thermal conductivity detector and a Pora PLOT Q column until steady state (up to 24 h).

Results and discussion

MIL-101(Cr) and MOF-199 were synthesized according to previously reported procedures with product identity established by powder X-ray diffraction (Fig. S2 and S3 in ESI†).[31,32,38,39] BET surface areas were 2770 m^2 g^{-1} and 950 m^2 g^{-1}, respectively. Particles sizes were in the range of 100–400 nm for MIL-101(Cr) and mostly below 100 nm except for some bigger crystals of about 400 nm for MOF-199 (Fig. 1). The prepared MOF particles were used to fabricate membranes with the 6FDA-*m*PD polyimide (see ESI†). From the scanning electron microscopy (SEM) cross-sections of the MOF@6FDA-*m*PD MMMs it is evident that the MOF particles showed excellent adhesion with the polymer matrix as the membrane cross-section morphology reveals the formation of circular cavities and elongated matrix segments with increased plastic deformation of the polymer (Fig. 2). The good interaction of the MOFs with the polymer is favored due to the partial organic nature of the former.

Interfacial voids were absent in the MMMs and MOF crystals were homogeneously distributed in the 6FDA-*m*PD matrix. No particle agglomeration can be observed. The X-ray patterns (Fig. S2 and S3 in ESI†) reveal that most of the main MOF reflections are present in the composite membranes. This also proves that the membrane preparation procedure did not alter the filler crystallinities. Furthermore, SEM images combined with elemental EDX mapping of chromium (MIL-101(Cr)) and copper (MOF-199) of the cross-sections of the MMMs (Fig. S3 and S5†) show also a remarkable homogeneous distribution of the MOF particles in the polymer matrix. Possible defects concerning particle agglomeration or particle sedimentation can thus be eliminated.

The gain of this MMM study is clearly demonstrated from the point of view of gas separation performance for CO_2/CH_4 gas mixtures (related to natural gas upgrading by removal of CO_2). Results of CO_2 and CH_4 gas permeation and separation experiments conducted with pure 6FDA-*m*PD membrane, MIL-101(Cr)@6FDA-*m*PD and MOF-199@6FDA-*m*PD MMMs are shown in Fig. 3 (data in Tables S2 and S3 in ESI†). Two to three membranes of each type were fabricated and every mem-

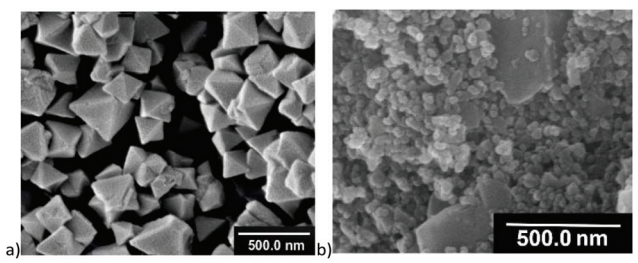

Fig. 1 Scanning electron microscopy (SEM) images of (a) MIL-101(Cr) and (b) MOF-199 nano/microcrystals.

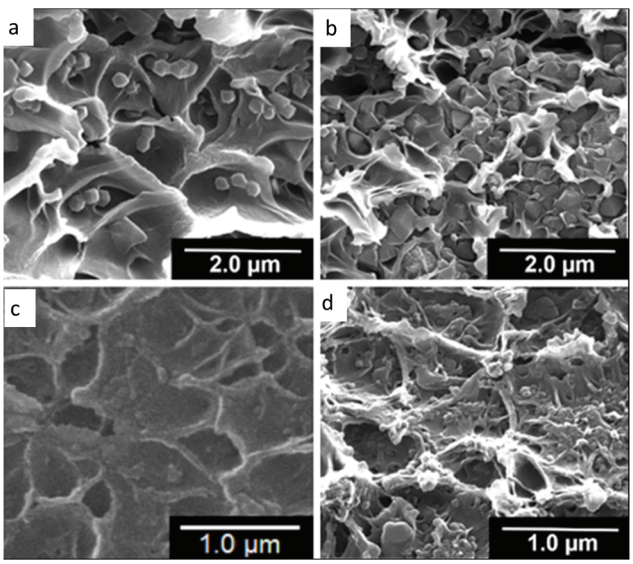

Fig. 2 SEM cross-sections of MOF@6FDA-*m*PD membranes based on 250 mg of 6FDA-*m*PD with different loadings of MOFs: (a) 8 wt% MIL-101(Cr), (b) 24 wt% MIL-101(Cr), (c) 8 wt% MOF-199 and (d) 24 wt% MOF-199.

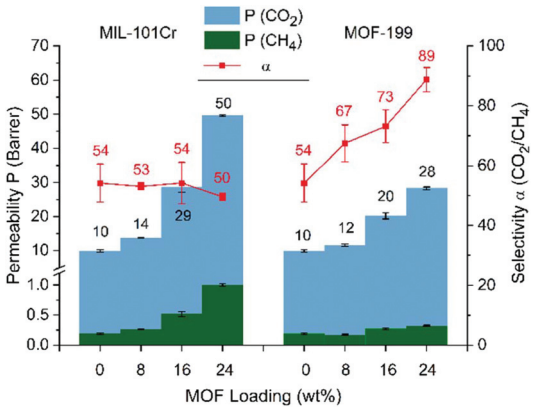

Fig. 3 CO_2/CH_4 permeability and separation performance of pure 6FDA-*m*PD (0 wt% MOF loading), MIL-101(Cr)@6FDA-*m*PD and MOF-199@6FDA-*m*PD MMMs at different MOF loadings. See Tables S2 and S3 in ESI† for experimental details.

brane was measured at least two times to provide reliable error estimates.

The gas separation experiments were performed at 25 °C and 35 °C, 4 and 3 bar feed pressure, respectively, and 50/50 CO_2/CH_4 mixture on MMMs containing 8, 16 and 24 wt% of either MIL-101(Cr) or MOF-199. These mixed-gas separation experiments indicated enhancements in CO_2 permeability with increasing MOF weight percentage in 6FDA-*m*PD. For all MIL-101(Cr)@6FDA-*m*PD MMMs the selectivity approximately remained equal to that of the neat polymer, while MOF-199@6FDA-*m*PD MMMs featured a steady rise in selectivity with increasing amount of MOF. This suggests that the membranes are free of interfacial defects, which otherwise would have led to a distinct decrease on the selectivity. The CO_2 permeability increased from about 10 Barrer for pure 6FDA-*m*PD to 50 or 28 Barrer in MMMs containing 24 wt% of MIL-101(Cr) or MOF-199, respectively. The CO_2/CH_4 selectivity decreased slightly from 54 for pure 6FDA-*m*PD to 50 for 24 wt% MIL-101(Cr)@6FDA-*m*PD MMM and increases significantly to 89 for 24 wt% of MOF-199@6FDA-*m*PD MMM (Fig. 3, data in Tables S2 and S3 in ESI†). Thus, the MMMs made of 6FDA-*m*PD and MIL-101(Cr) or MOF-199 provide a remarkable gas-separation performance enhancement as compared with the pure polyimide with respect to permeability or selectivity, respectively.

The breaking of polymer chain packing and linking due to the presence of fillers leading to an increase in polymer matrix free volume and especially the large porosity of MOFs can explain the permeability improvement in agreement with previous publications related to ZIF-8 or Al-fumarate containing MMMs.[40,41]

A rigidification of polymer chains in the composite membranes does not occur as the T_g, determined by differential scanning calorimetry, decreases slightly for the MOF-199@6FDA-*m*PD MMMs compared to the neat polymer (Table S4†). For MIL-101(Cr)@6FDA-*m*PD MMMs the T_g exhibits no distinct trend for a rigidification or disruption of polymer chains.

For most composite membranes, a constant selectivity is observed with increased MOF loading, as is found here for the MIL-101(Cr)@6FDA-*m*PD MMMs.[10,42] Therefore, the increase in selectivity for MOF-199@6FDA-*m*PD MMMs contrasts with expectations since the used MOFs have large cages and window sizes in their neat, virgin state, and no size exclusion of any gas from CO_2/CH_4 mixtures is likely if the MOF would remain unchanged. According to literature MIL-101(Cr) has cages with diameters of 3.4 nm and hexagonal windows of 1.6 nm diameter.[31] MOF-199 has square channels of 9 × 9 Å with 13 Å across the diagonals.[39]

In some cases, where a selectivity increase has been seen with MOF@polymer composite membranes, the following reasons were given for the increase in selectivity.

- The polymer could be influenced by the filler in such a way, that a chain rigidification takes places which results in a higher T_g for the composite membrane in comparison to the pure polymer membrane. The general correlation of the T_g of the polymer with permeability and selectivity is, that a high T_g goes together with low permeability and high selectivity and *vice versa*.[43]

- The MOF filler could become size discriminating if the polymer chains diffuse through the MOF channels and block them to some degree. This blocking can intensify the molecular sieving property of the MOF and enhance transport of smaller gas molecules relative to the larger ones and thereby induce a higher selectivity.[48]

- MOF fillers, such as ZIF-8, with pore apertures of ~4 Å feature sieving properties based on their diffusion selectivity even for gas pairs with kinetic diameters of <4 Å if they are properly matched with the polymer matrix.[44]

- The MOF filler could show a very high adsorption affinity for one specific gas and thus increases the transport of this gas through the membrane, which can also result in an increased selectivity.[45,46]

In our case an increase in T_g was clearly not observed, but rather a decrease in the T_g was measured. Thus, the increase in selectivity cannot be due to the change in polymer structure alone. At the same time MOFs by itself, as for example in pure MOF membranes are not known for high selectivities.[47]

The apparent increase in selectivity for the MOF-199 MMMs may be due to the fact, that the polyimide blocked or partially reduced the access to the MOF-199 channels. Whereby the MOF filler becomes more size discriminating, that is exhibits intensified molecular sieving properties through the enhanced transport of smaller gas molecules relative to the larger ones which leads to a higher selectivity. CO_2 and CH_4 have kinetic diameters of 0.33 and 0.38 nm, respectively.

Furthermore, the increase in CO_2/CH_4 selectivity for MOF-199@6FDA-*m*PD MMMs may also be promoted by the high adsorption efficiency of MOF-199 for CO_2 (see above).[36]

Moreover, the good dispersion and non-agglomeration of MOF-199 particles may favor the action of adsorbing CO_2 over CH_4 improving the separation selectivity up to the total loading of 24 wt%.[48] Likewise, an increased selectivity for

different MOF-199@polymer MMMs with increasing MOF content was observed. The selectivity increase for MOF-199@poly(vinylidene fluoride) (PVDF) was from 21 to 40 when going from neat PVDF to 15 wt% MOF content.[49] For MOF-199@Matrimid the increase was from 17 to 23 when going from neat Matrimid to 30 wt% MOF content (see also Table S5†).[50] This effect was especially evident for small MOF-199 particles in the nanometer range, which in this study were also used, due to better distribution in the polymer matrix and neglectable formation of voids between MOF particles.[45,51]

The difference in gas separation performances between the fabricated MMMs result from the varying structure and properties of the MOFs. MIL-101(Cr) exhibits a much higher pore volume of about 1.32 $cm^3\ g^{-1}$ compared to the pore volume of 0.78 $cm^3\ g^{-1}$ of MOF-199. Hence, the density of MIL-101(Cr) is much lower, which leads to a considerably higher volume fraction for the same amount of loaded wt% for MIL-101(Cr) in the MMMs (see eqn (S2), ESI† how ϕ_d is derived from the MOF loading in wt%). Thus, the increase in free volume is more pronounced for the MIL-101(Cr)@6FDA-*m*PD MMMs, which ultimately leads to the higher permeability in comparison to the MOF-199@6FDA-*m*PD MMMs.[41] This observation is in good agreement with the results emerging from the Maxwell model for CO_2, shown in Fig. 4a, which was applied to both types of MMMs.

The Maxwell model with the assumption $P_d \gg P_c$, (eqn (1)) is a highly specialized limiting version of the full Maxwell model, which can be designated as "Maxwell model ∞". This limiting case corresponds essentially to the introduction of infinitely permeable voids with a volume fraction equal to that of the dispersed phase.

$$P_d \gg P_c;\ \frac{P_{eff}}{P_c} = \frac{1 + 2\phi_d}{1 - \phi_d} \quad (1)$$

The "Maxwell model ∞" with the assumption $P_d \gg P_c$, that is, an infinite high CH_4 permeability of the dispersed, filler phase does not give a good agreement with the experimental data. The latter stays below the predicted line of the "Maxwell model ∞" (Fig. 4b). In reverse conclusion this indicates that the assumption $P_d \gg P_c$ is no longer valid for CH_4 and MOF-199. Instead the relative experimental permeability approaches the Maxwell model with $P_d = P_c$.

Since in pure MOF-199 the CH_4 permeability (from single-gas permeation) was 1000 Barrer, we have to conclude that either pore blocking from polymer chain ends results in discriminating CH_4 from entering the pores or that the excellent adsorption of CO_2 compared to CH_4 in MOF-199 prevents CH_4 from entering the pores (see above).

As Fig. 4 indicates, the filler volume of the 16 wt% MIL-101 (Cr)-6FDA-*m*PD MMMs already surpasses the filler volume of the 24 wt% MOF-199@6FDA-*m*PD MMM and as a consequence the relative permeability of the 16 wt% MIL-101(Cr) MMM already reaches the is the relative permeability of the MOF-199 MMM. In general, one can observe a good match between the predicted values of the "Maxwell model ∞" for the composite membranes and the experimental values. Larger deviations between the model and the experimental values are revealed for higher loadings of a filler volume fraction ϕ_d above 0.4 and

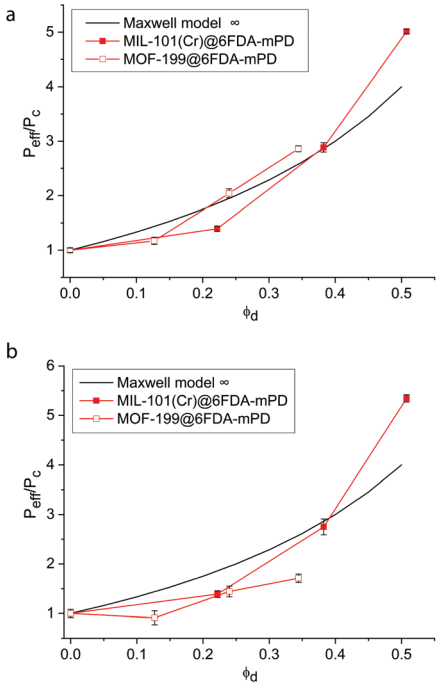

Fig. 4 Relative experimental (a) CO_2 and (b) CH_4 permeabilities (referenced to the permeability P_c of the pure polymer membrane) for MIL-101(Cr)@6FDA-*m*PD MMMs (filled red squares) and MOF-199@6FDA-*m*PD MMMs (hollow red squares) with different filler volume fraction ϕ_d (see eqn (S2), ESI† how ϕ_d is derived from the MOF loading in wt%). The black line gives the relative theoretical gas permeabilities for a porous filler (with permeability $P_d \gg P_c$). Note that for the same wt% of MOF the higher density MOF-199 leads to a lower filler volume fraction (see ESI† for details to the Maxwell model).

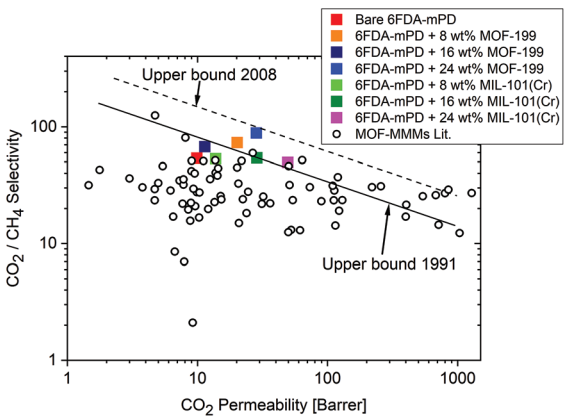

Fig. 5 CO_2/CH_4 separation performance of the studied MOF@6FDA-*m*PD MMMs compared with the results from previously reported MOF MMMs (see Table S5†). The straight lines are the Robeson upper bounds for best polymer separation performances as defined in 1991[8] and 2008.[18]

should result from filler–filler interactions which are not considered in the Maxwell model.[52]

In Fig. 5 we compare the presented results with those previously reported from other MOF-containing MMMs (see Table S5†). The performance of the 6FDA-*m*PD membrane with 8 wt% of MIL-101(Cr) is located in the region considered as commercially unattractive. However, the performance of MOF-199@6FDA-*m*PD MMMs with 24 wt% MOF loading clearly surpasses the polymer upper bound drawn in 1991, and reaches the commercially attractive region. A MOF-199@6FDA-*m*PD membrane with 24 wt% MOF loading exhibits specifically much higher CO_2/CH_4 mixed-gas selectivity (89) than most other MOF-based MMMs, combined with a good CO_2 permeability of 28 Barrer.

Conclusions

In summary, high-performance gas separation mixed-matrix membranes were obtained by combining the polyimide 6FDA-*m*PD and nano- to microcrystalline particles of the MOFs MIL-101(Cr) or MOF-199 (HKUST-1, Cu-BTC). The MOF particles showed good adhesion with the polymer matrix and the resulting membranes were free of interfacial defects. We demonstrated that the MMMs yielded to a substantial increase in CO_2 permeability as well as in CO_2/CH_4 selectivity for the MOF-199@6FDA-*m*PD MMMs. The high permeability increase for the MIL-101(Cr)@6FDA-*m*PD MMMs can be traced to the high pore volume in MIL-101(Cr). The remarkable and unexpected increase in selectivity for the MOF-199 MMMs is reasoned by pore blocking and reduction of the MOF window size through polyimide together with the high adsorption of CO_2 by MOF-199. Still, more investigations are necessary for better elucidation of permeation mechanisms and selectivity properties, the intrinsic gas-transport properties of MOFs, the roles of filler loading, geometry, pore size and the nature of the molecular interactions on preferential adsorption when using MOFs in MMMs.

Conflicts of interest

There are no conflicts to declare.

Acknowledgements

Financial support (MAT2013-40556-R) from the Ministry of Economy and Competitiveness (MINECO) is gratefully acknowledged by JC. The work of CJ was supported by the Federal German Ministry of Education and Research (BMBF) under grant Optimat 03SF0492C. We thank Mrs Alexa Schmitz for TGA and Mr Carsten Schlüsener for SEM/EDX measurements.

Notes and references

1 J. C. Davis, R. J. Valus, R. Eshragi and A. E. Velikoff, *Sep. Sci. Technol.*, 1993, **28**, 463–476.
2 M. G. Buonomenna, *RSC Adv.*, 2013, **3**, 5694–5740.
3 J. C. Charpentier, *Chem. Eng. J.*, 2007, **134**, 84–92.
4 W. J. Koros, *AIChE J.*, 2004, **50**, 2326–2334.
5 J. Coronas and J. Santamaria, *Sep. Purif. Methods*, 1999, **28**, 127–177.
6 M. A. Aroon, A. F. Ismail, T. Matsuura and M. M. Montazer-Rahmati, *Sep. Purif. Technol.*, 2010, **75**, 229–242.
7 T. S. Chung, L. Y. Jiang, Y. Li and S. Kulprathipanja, *Prog. Polym. Sci.*, 2007, **32**, 483–507.
8 L. M. Robeson, *J. Membr. Sci.*, 1991, **62**, 165–185.
9 B. Zornoza, A. Martinez-Joaristi, P. Serra-Crespo, C. Tellez, J. Coronas, J. Gascon and F. Kapteijn, *Chem. Commun.*, 2011, **47**, 9522–9524.
10 J. Dechnik, C. J. Sumby and C. Janiak, *Cryst. Growth Des.*, 2017, **17**, 4467–4488; J. Dechnik, J. Gascon, C. J. Doonan, C. Janiak and C. J. Sumby, *Angew. Chem., Int. Ed.*, 2017, **56**, 9292–9310.
11 O. G. Nik, X. Y. Chen and S. Kaliaguine, *J. Membr. Sci.*, 2012, **413–414**, 48–61.
12 H. B. Tanh Jeazet, C. Staudt and C. Janiak, *Dalton Trans.*, 2012, **41**, 14003–14027; K. Hunger, N. Schmeling, H. B. Tanh Jeazet, C. Janiak, C. Staudt and K. Kleinermanns, *Membranes*, 2012, **2**, 727–763; H. B. Tanh Jeazet and C. Janiak, Metal-Organic Frameworks in Mixed-Matrix Membranes, in *Metal Organic Framework Materials*, ed. L. R. MacGillivray and C. Lukehart, John Wiley & Sons, Ltd, Chichester, UK, 2014, pp. 1–15.
13 B. Zornoza, C. Tellez, J. Coronas, J. Gascon and F. Kapteijn, *Microporous Mesoporous Mater.*, 2013, **166**, 67–78.
14 D. Bastani, N. Esmaeili and M. Asadollahi, *J. Ind. Eng. Chem.*, 2013, **19**, 375–393.
15 G. Dong, H. Li and V. Chen, *J. Mater. Chem. A*, 2013, **1**, 4610–4630.
16 M. J. C. Ordonez, K. J. Balkus, Jr., J. P. Ferraris and I. H. Musselman, *J. Membr. Sci.*, 2010, **361**, 28–37.
17 Y. Dai, J. R. Johnson, O. Karvan, D. S. Sholl and W. J. Koros, *J. Membr. Sci.*, 2012, **401–402**, 76–82; D. Zheng, X. Liu, D. Hu, M. Li, J. Zhang, G. Zeng, Y. Zhang and Y. Sun, *RSC Adv.*, 2014, **4**, 10140–10143; M. G. Buonomenna, W. Yave and G. Golemme, *RSC Adv.*, 2012, **2**, 10745–10773; X. Y. Chen, H. Vinh-Thang, D. Rodrigue and S. Kaliaguine, *RSC Adv.*, 2014, **4**, 12235–12244; S. Sorribas, B. Zornoza, C. Téllez and J. Coronas, *J. Membr. Sci.*, 2014, **452**, 184–192; P. Burmann, B. Zornoza, C. Téllez and J. Coronas, *Chem. Eng. Sci.*, 2014, **107**, 66–75; X. Y. Chen, H. Vinh-Thang, D. Rodrigue and S. Kaliaguine, *Ind. Eng. Chem. Res.*, 2012, **51**, 6895–6906; B. Seoane, J. M. Zamaro, C. Téllez and J. Coronas, *RSC Adv.*, 2011, **1**, 917–922; X. Y. Chen, H. Vinh-Thang, D. Rodrigue and S. Kaliaguine, *RSC Adv.*, 2013, **3**, 24266–24279.
18 L. M. Robeson, *J. Membr. Sci.*, 2008, **320**, 390–400.

19 G. Rebollar-Perez, E. Carretier, N. Lesage and P. Moulin, *Membranes*, 2011, **1**, 80–90.
20 L. Dumee, L. Velleman, K. Sears, M. Hill, J. Schutz, N. Finn, M. Duke and S. Gray, *Membranes*, 2011, **1**, 25–36.
21 P. S. Goh, A. F. Ismail, S. M. Sanip, B. C. Ng and M. Aziz, *Sep. Purif. Technol.*, 2011, **81**, 243–264.
22 B. Seoane, J. Coronas, I. Gascon, M. E. Benavides, O. Karvan, J. Caro, F. Kapteijn and J. Gascon, *Chem. Soc. Rev.*, 2015, **44**, 2421–2454.
23 R. D. Noble, *J. Membr. Sci.*, 2011, **378**, 393–397.
24 J.-R. Li, Y. Ma, M. C. McCarthy, J. Sculley, J. Yu, H.-K. Jeong, P. B. Balbuena and H.-C. Zhou, *Coord. Chem. Rev.*, 2011, **255**, 1791–1823.
25 D. Liu and C. Zhong, *J. Mater. Chem.*, 2010, **20**, 10308–10318.
26 S. T. Meek, J. A. Greathouse and M. D. Allendorf, *Adv. Mater.*, 2011, **23**, 249–267.
27 T.-H. Bae, J. S. Lee, W. Qju, W. J. Koros, C. W. Jones and S. Nair, *Angew. Chem., Int. Ed.*, 2010, **49**, 9863–9866.
28 C. Janiak and J. K. Vieth, *New J. Chem.*, 2010, **34**, 2366–2388.
29 S. Keskin and D. S. Sholl, *Energy Environ. Sci.*, 2010, **3**, 343–351; J. A. Sheffel and M. Tsapatsis, *J. Membr. Sci.*, 2009, **326**, 595–607.
30 S. Aguado, J. Canivet and D. Farrusseng, *J. Mater. Chem.*, 2011, **21**, 7582–7588.
31 G. Férey, C. Mellot-Draznieks, C. Serre, F. Millange, J. Dutour, S. Surble and I. Margiolaki, *Science*, 2005, **309**, 2040–2042.
32 D. J. Tranchemontagne, J. R. Hunt and O. M. Yaghi, *Tetrahedron*, 2008, **64**, 8553–8557.
33 C. Staudt-Bickel and W. J. Koros, *J. Membr. Sci.*, 1999, **155**, 145–154.
34 K. Sumida, D. L. Rogow, J. A. Mason, T. M. McDonald, E. D. Bloch, Z. R. Herm, T.-H. Bae and J. R. Long, *Chem. Rev.*, 2012, **112**, 724–781; Z. Zhang, Y. Zhao, Q. Gong, Z. Li and J. Li, *Chem. Commun.*, 2013, **49**, 653–661; J. Liu, P. K. Thallapally, B. P. McGrail, D. R. Brown and J. Liu, *Chem. Soc. Rev.*, 2012, **41**, 2308–2322; X. Lu, D. Jin, S. Wei, Z. Wang, C. An and W. Guo, *J. Mater. Chem. A*, 2015, **3**, 12118–12132.
35 A. Khutia and C. Janiak, *Dalton Trans.*, 2014, **43**, 1338–1347.
36 A. Ö. Yazaydin, A. I. Benin, S. A. Faheem, P. Jakubczak, J. L. Low, R. R. Willis and R. Q. Snurr, *Chem. Mater.*, 2009, **21**, 1425–1430.
37 B. Zornoza, S. Irusta, C. Tellez and J. Coronas, *Langmuir*, 2009, **25**, 5903–5909; S. Sorribas, B. Zornoza, C. Téllez and J. Coronas, *J. Membr. Sci.*, 2014, **452**, 184–192.
38 T. Zhao, F. Jeremias, I. Boldog, B. Nguyen, S. K. Henninger and C. Janiak, *Dalton Trans.*, 2015, **44**, 16791–16801; A. Herbst, A. Khutia and C. Janiak, *Inorg. Chem.*, 2014, **53**, 7319–7333.
39 S. S.-Y. Chui, S. M.-F. Lo, J. P. H. Charmant, A. G. Orpen and I. D. Williams, *Science*, 1999, **283**, 1148–1150.
40 B. Zornoza, B. Seoane, J. M. Zamaro, C. Téllez and J. Coronas, *ChemPhysChem*, 2011, **12**, 2781–2785.
41 A. Nuhnen, D. Dietrich, S. Millan and C. Janiak, *ACS Appl. Mater. Interfaces*, 2018, **10**, 33589–33600.
42 A. E. Amooghin, S. Mashhadikhan, H. Sanaeepur, A. Moghadassi, T. Matsuura and S. Ramakrishna, *Prog. Mater. Sci.*, 2019, **102**, 222–295.
43 Y. Li, T.-S. Chung, C. Cao and S. Kulprathipanja, *J. Membr. Sci.*, 2005, **260**, 45–55.
44 W. J. Koros and C. Zhang, *Nat. Mater.*, 2017, **16**, 289–297.
45 N. M. Jacques, P. R. E. Rought, D. Fritsch, M. Savage, H. G. W. Godfrey, L. Li, T. Mitra, M. D. Frogley, G. Clinque, S. Yang and M. Schröder, *Chem. Commun.*, 2018, **54**, 2866–2869.
46 R. Abedini, A. Mosayebi and M. Mokhtari, *Process Saf. Environ. Prot.*, 2018, **114**, 229–239.
47 S. Qiu, M. Xue and G. Zhu, *Chem. Soc. Rev.*, 2014, **43**, 6116–6140.
48 H. W. B. Teo, A. Chakraborty and S. Kayal, *Appl. Therm. Eng.*, 2017, **110**, 891–900.
49 E. A. Fejani, H. Mahdavi and A. Tavasoli, *Chem. Eng. Res. Des.*, 2015, **96**, 87–102.
50 S. Basu, A. Cano-Odena and I. F. J. Vankelecom, *Sep. Purif. Technol.*, 2011, **81**, 31–40.
51 R. Lin, L. Ge, H. Diao, V. Rudolph and Z. Zhu, *ACS Appl. Mater. Interfaces*, 2016, **8**, 32041–32049.
52 R. H. B. Bouma, A. Checchetti, G. Chidichimo and E. Drioli, *J. Membr. Sci.*, 1997, **128**, 141–149.